RESEARCH ARTICLE

Thermodynamics and Molecular-Scale Phenomena

Phase behavior of ionic fluid in charged confinement: An associating polymer density functional theory study

Jin Cheng[1] | Jipeng Xu[1] | Sijie Wang[1] | Xueqian Chen[2] | Cheng Lian[1] ⓘ | Honglai Liu[1]

[1]State Key Laboratory of Chemical Engineering, Shanghai Engineering Research Center of Hierarchical Nanomaterials, Frontiers Science Center for Materiobiology and Dynamic Chemistry, and School of Chemistry and Molecular Engineering, East China University of Science and Technology, Shanghai, China

[2]School of Physics, East China University of Science and Technology, Shanghai, China

Correspondence
Cheng Lian and Honglai Liu, State Key Laboratory of Chemical Engineering, Shanghai Engineering Research Center of Hierarchical Nanomaterials, Frontiers Science Center for Materiobiology and Dynamic Chemistry, and School of Chemistry and Molecular Engineering, East China University of Science and Technology, Shanghai 200237, China.
Email: liancheng@ecust.edu.cn and hlliu@ecust.edu.cn

Funding information
State Key Laboratory of Clean Energy Utilization, Grant/Award Number: ZJUCEU2021005; National Key Research and Development Program of China, Grant/Award Number: 2022YFA1503501; Fundamental Research Funds for the Central Universities, Grant/Award Number: 2022ZFJH004; 21C Innovation Laboratory, Contemporary Amperex Technology Ltd, Grant/Award Number: 21C-368 OP-202312; National Natural Science Foundation of China, Grant/Award Number: 22278127

Abstract

With the rapid advancement of the new energy industry, porous electrode materials and complex electrolytes have gained widespread usage. Electrolytes exhibit distinctive phase behavior when subjected to the combined influence of confined space and electric fields. However, the measurement and prediction of such phase behavior encounter significant challenges. Consequently, numerous theoretical tools have been employed to establish models for phase equilibrium calculations. Nevertheless, current research in this field has notable limitations and fails to address the confinement of space or complex polymer electrolytes. Considering these shortcomings, an associating polymer density functional theory (PDFT) was developed by modifying excess free energy. This study examines the phase behavior of electrolytes with various chain lengths within diverse confined slits, revealing that the confinement effect and fluid tail chains can narrow the phase diagram. Additionally, a linear correlation between the electric field strength and the phase equilibrium offset has been identified, and a quantitative relationship is derived. The results of this investigation contribute to a deeper comprehension of complex fluid phase behavior and guide the design of electrochemical devices.

KEYWORDS
electrolyte, phase behavior, phase diagram, polymer density functional theory, porous electrode

1 | INTRODUCTION

With the rapid development of the new energy industry, many new electrochemical energy storage devices have been developed and widely used.[1-3] The performance of electrochemical modules is closely related to the micro-interface structure.[4-7] In recent years, with new electrolytes and electrode materials, novel electrochemical interfaces have emerged,[8-10] which are more complex than the previous microenvironment and lead to further problems.[11-13] Complex electrolytes are bound to exhibit unique phase behavior in porous electrode materials or battery separators under the dual effects of confined space and electric field.[14,15] Many slits in the battery are only a few nanometers wide, and the electrolytes used are not just ordinary ions but may be complex ionic liquids or polymers.[16-18] Monte Carlo (MC) simulation has shown that the first-order phase transition may occur in porous electrodes when the pore

size is equivalent to the ion size.[19-21] Different phase behaviors will affect the performance of electrochemical modules.[22,23] However, due to the experimental difficulties in accurately describing the phase behavior, the phase diagram under special conditions cannot be measured. For complex fluids, such problems are more prominent.[24,25] Therefore, the phase behavior of complex fluid in confined charged space is a difficult problem.

Previously, many scholars have explored the phase behavior of complex electrolytes and drawn many phase diagrams.[26-28] At first, it mainly used experimental methods, including phase diagrams and critical points of various ionic liquids, aromatic compounds, alkanes, etc.[29,30] They also explored the influence of special effects, such as the benzene fluoride effect, which makes the binary mixture of ionic liquid and benzene or its derivatives show an unusual phase diagram.[31] These studies reveal the phase behavior of complex fluids, but there are still many deficiencies. Only specific fluids and homogeneous phase diagrams can be processed.

Due to the difficulties of experimental measurement in special environments such as confined spaces, some scholars began to use theoretical tools to explore the phase behavior under complex conditions.[32,33] The most classical phase equilibrium theory method is MC simulation. Early MC was widely used in complex fluid phase equilibrium, including gas-liquid and liquid-liquid equilibrium of polymers.[34-36] Later, some scholars built complex molecular thermodynamic models. The equation of state is established based on Freed's theory and Flory-Huggins's theory.[37-40] They can also obtain excellent phase behavior prediction results by correlating critical points. Later, Kondrat et al.[41] began to pay attention to the fluid density functional theory (FDFT) and introduced it into the study of phase behavior, such as the phase behavior of ionic liquid crystals. After that, Liu et al. noticed the advantages of FDFT and began to improve it and apply it to study the phase behavior of confined space and asymmetric electrolytes. They calculated many phase diagrams, revealing the effects of restrictions, voltage, asymmetry, and other factors on phase equilibrium.[42,43] However, due to the limitation of the theory and calculation program, this work can only deal with simple ions, which is too simple for ionic liquids often used in practical applications. Ions can only be represented by a single hardball, and the chain structure of some electrolytes cannot be reflected, so there are great obstacles in application. Therefore, a general molecular thermodynamic model is urgently needed to accurately and quickly describe the distribution and phase behavior of various complex fluids in confined, charged, and other situations.[44]

In this work, we modified the excess free energy based on the previous polymer density functional theory (PDFT),[45-49] which is an extension method based on FDFT, so that it can simultaneously consider the chain connection and ion association effects, and proposed the associating PDFT. The phase equilibrium of ionic liquids with different chain lengths in confined spaces with different widths is studied. The gas-liquid equilibrium phase diagrams of different electrolytes can be drawn by adjusting the temperature, and the critical point can be found. Due to the use conditions of electrolytes mostly existing in electric fields, this work also studies the phase equilibrium in confined

space under different electric fields and finds the empirical rule of electric field on phase diagram offset. This study is structured as follows. First, we establish the associating PDFT to describe ionic liquids with variable chain lengths using a coarse-grained model. Second, we provide a brief introduction to the PDFT and the relevant parameters used in this work. Subsequently, we discuss the impact of different ionic liquid chain lengths and slit width on phase equilibrium and find the relationship between different potential and phase diagram offsets. Finally, we summarize the main findings and highlight the potential implications for future research.

2 | MODEL AND METHODS

2.1 | Molecular model

As shown in Figure 1, we establish a coarse-grained model of ionic liquids with different chain lengths in a confined system. An ionic fluid in the bulk may exist either as a liquid-like or as a vapor-like (or two liquids with different ionic densities) in slit pores. Similar to previous studies.[45,50,51] Ions are coarsened into hard spheres of the same size. Anions will be connected by a neutral segment with different lengths, representing different ionic liquids. The tail chain length 0-2 is selected for the commonly used ionic liquids. Theoretically, the PDFT is universal and can also study ions of other sizes and longer chains. The diameters of anions, neutral segments, and cations are all set to 0.5 nm. To maintain simplicity and efficiency within the model, the theory simplifies molecular details and does not consider interactions at the atomic and electronic scale.

2.2 | Polymer density functional theory

FDFT is a general statistical mechanics method applicable to grand canonical ensembles, which can describe the structure and thermodynamic properties of fluid from a molecular perspective.[44,47,52] By constructing the free energy and calculating the functional variation of the density distribution function, the microstructure and macroscopic thermodynamic properties of the system equilibrium state can be obtained. The essence of FDFT calculation is to obtain the Euler–Lagrange equation and obtain the relationship between the density distribution function $\rho(r)$ driven by chemical potential μ and the position r. The PDFT is a further extension of FDFT, incorporating considerations for the connectivity of polymer chains. The excess Helmholtz free energy caused by the chain connectivity of polymer fluids can be described using the corresponding monomer system as a reference through perturbation theory. Previous studies[53,54] have established the groundwork for PDFT calculations. It is assumed that the density distribution curve varies solely in the z-direction, which is perpendicular to the electrode plate. The fundamental concept behind PDFT is the minimization of the grand potential. Consequently, the one-dimensional density profiles can be projected.

FIGURE 1 Schematic depiction of the phase separation phenomenon occurring in a confined slit pore for an ionic fluid. The studied system includes three types of ionic fluids.
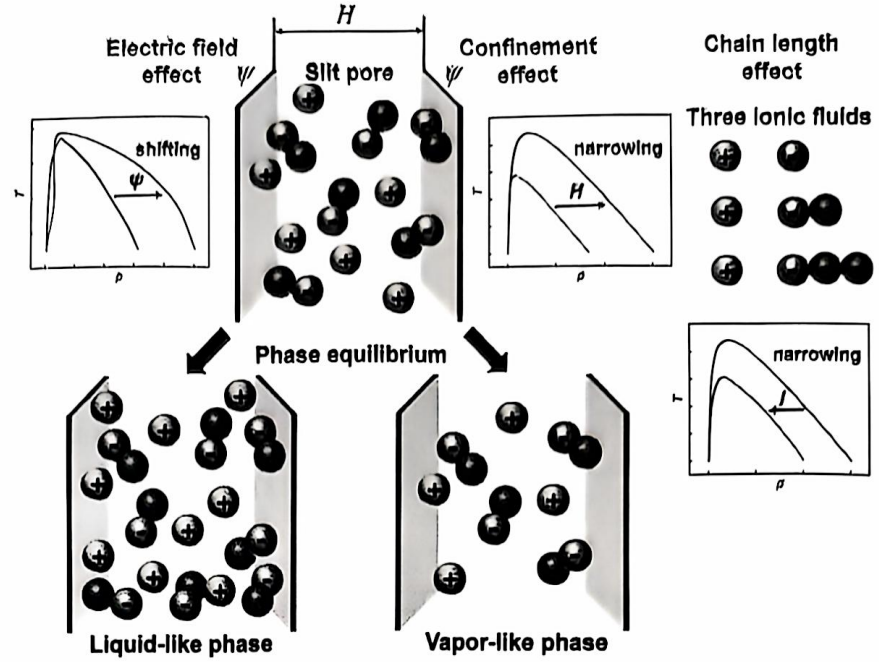
$$\beta\Omega[\rho_M(R),\{\rho_c(r)\}] = \beta F[\rho_M(R),\{\rho_c(r)\}]$$
$$+ \int[\beta\Psi_M(R) - \beta\mu_M]\rho_M(R)dR \qquad (1)$$
$$+ \sum_c \int[\beta\Psi_c(r) - \beta\mu_c]\rho_c(r)dr$$

Here, $\beta^{-1} = k_BT$, R represents the coordinates that specify the position of each cationic hard sphere. μ_c and μ_M indicate the chemical potentials, respectively. $\Psi_M(R)$ specifically referred to as $\Psi_M(R) = \sum_{i=1}^{m}\varphi_i(r_i)$. Finally, F denotes the Helmholtz energy, which encompasses contributions from both ideal gas behavior and excess intermolecular interactions F^{ex}.

$$\beta F = \int[\ln\rho_M(R) - 1]\rho_M(R)dR + \beta\int V_b(R)\rho_M(R)dR$$
$$+ \sum_c \int[\ln\rho_c(r) - 1]\rho_c(r)dr + \beta F^{ex} \qquad (2)$$

Through the decomposition of the ideal and non-ideal parts of the Helmholtz free energy to minimize the grand potential Ω, in Equation (1). It is possible to derive the Euler-Lagrange equations for the density profiles of both polymers and monomers segmented into distinct sections. These equations are critical for analyzing the behavior of the system.

$$\rho_M(R) = \exp\left[\beta\mu_M - \beta V_b(R) - \beta\Psi_M(R) - \frac{\delta\beta F^{ex}}{\delta\rho_M(R)}\right]$$
$$\rho_c(r) = \exp\left[\beta\mu_c - \beta\Psi_c(r) - \frac{\delta\beta F^{ex}}{\delta\rho_c(r)}\right] \qquad (3)$$

The density profiles of negatively charged anionic segments and segments with no charge can be obtained:

$$\rho_m(r_m) = \int dR\delta(r - r_m)\rho_M(R) \qquad (4)$$

Among these segments, the negative segments represent $1/m$. Using Equations (3) and (4), the calculations for each part can be performed accurately.

2.3 | Excess free energy functional of associating PDFT

The majority of previous applications of PDFT in ion systems rely on the use of excess intrinsic Helmholtz energy, which is typically obtained through the utilization of diverse mean-spherical approximation (MSA). The methods can produce reasonably accurate predictions of ionic density profiles when compared to simulation data, MSA presents significant limitations in its ability to describe the bulk phase behavior of ionic fluids. Specifically, it fails to reproduce the observed liquid-vapor coexistence from the virial or compressibility equations of state, and its predictions for the critical temperature and density through the energy route exhibit severe deviations from values obtained through molecular simulations. Recent studies have demonstrated that the application capability of MSA can be greatly enhanced by incorporating associations between ions with opposite charges.

To make the theory applicable to complex chain-like fluids, we propose a theoretical scheme associating PDFT in this work, in which MSA is used to explain the electrostatic correlation, and thermodynamic perturbation theory (TPT) is used to express the correlation between ions with opposite charges, taking chain connectivity into account. The F^{ex} can be written as

$$F^{ex} = F_{hs}^{ex} + F_C^{ex} + F_{el}^{ex} + F_{ch}^{ex} + F_{as}^{ex}. \qquad (5)$$

F_{ch}^{ex} and F_{as}^{ex} are introduced in detail as key points for theoretical improvements, and explicit expressions for other terms are provided

in Data S2. The excess chemical potential represents the change in the excess Helmholtz free energy due to a small variation in the density profiles,

$$\mu^{ex}(r) = \frac{\delta F^{ex}}{\delta \rho(r)} = \mu_{hu}^{ex}(r) + \mu_{ch}^{ex}(r) + \mu_{E}^{ex}(r) + \mu_{B}^{ex}(r) + \mu_{as}^{ex}(r). \quad (6)$$

The collective sum of these excess chemical potentials yields the total excess chemical potential.

2.3.1 | Chain connectivity based on first-order perturbation theory

The perturbation theory is employed to characterize the excess Helmholtz free energy arising from the chain connectivity of the polymer fluid, with the reference system being the corresponding monomer system. In the case of a homogeneous system, Wertheim[55] initially introduced the TPT to investigate hard-sphere molecules in relation to a monomer hard-sphere fluid. While TPT exists in various versions, we will provide a concise overview of the generalization of first-order TPT (TPT1) for inhomogeneous systems.

$$\beta\mu_{ch,l}^{ex}(r) = \frac{\delta\beta F_{ch}^{ex}}{\delta\rho_l(r)} = \sum_\alpha \int dr' \frac{\partial \Phi_{ch}^{ex}}{\partial n_{\alpha,l}(r')} \omega_l^{(\alpha)}(r' - r). \quad (7)$$

The free energy density, denoted as Φ_{ch}^{ex}, is determined based on the chain connectivity. It is worth noting that the existing literature[56,57] provides comprehensive equations specific to our system.

2.3.2 | Association between oppositely charged ions

The Helmholtz energy resulting from the interaction between ions of opposite charge is derived using the TPT1.[58]

$$\beta F_{as}^{ex}[\rho_l(r)] = \int dr \Phi^{as}[n_\alpha(r)], \quad (8)$$

where $\Phi^{as}[n_\alpha(r)]$ is given by

$$\Phi^{as}[n_\alpha(r)] = \sum_l n_{0,l}\zeta_l \left[\ln\alpha^{(l)}(r) - \frac{\alpha^{(l)}(r)}{2} + \frac{1}{2}\right]. \quad (9)$$

Like the methodology applied to association, $\alpha^{(l)}(r)$ is derived from

$$\alpha^{(l)}(r) = \frac{1}{1 + n_{0,l}\zeta_l\alpha^{(l)}(r)\Delta^{ij}(r)}, \quad (10)$$

where $\Delta^{ij}(r) = K^0 \times K'$.

The process of determining association constant K^0 involves a certain degree of arbitrary choice. The approach proposed by Ebeling[59] demonstrates an accurate prediction of the second ionic-virial coefficient. As noted in reference,[60] the selection of K^0 for this study is based on the proposal by Olaussen[61]

$$K^0 \approx 96\pi\sigma^3 \sum_{m=2}^{\infty} \frac{(T^*)^{-2m}}{(2m)!(2m-3)}. \quad (11)$$

The calculation of K' is performed using the straightforward interpolation scheme

$$K' = y_{+-}(\sigma)$$
$$= \left[\frac{1}{1-n_3} + \frac{n_2\sigma_+\sigma_-(1-n_{v2}n_{v2}/n_2^2)}{4\sigma_{+-}(1-n_3)^2}\right]\exp\left(-\frac{\Gamma^2\sigma_+\sigma_-}{4\pi^2 l_B\sigma_{+-}}\right)\exp\left(\frac{l_B Z_+ Z_-}{\sigma_{+-}}\right). \quad (12)$$

where $y_{+-}(\sigma)$ denotes the cavity correlation function for the contact between anion and cation, which is evaluated at $\alpha = 1$, representing the reference ionic fluid without association.

The excess chemical potential $\mu_{as,l}^{ex}(r)$, expressed as.

$$\beta\mu_{as,l}^{ex}(r) = \frac{\delta\beta F_{as}^{ex}}{\delta\rho_l(r)} = \sum_\alpha \int dr' \frac{\partial \Phi_{as}^{ex}}{\partial n_\alpha(r')} \omega_l^{(\alpha)}(r' - r). \quad (13)$$

2.4 | Grand potential and chemical potential

For a one-component open system, the grand partition function is given by

$$\Xi = \sum_{N=0}^{\infty} \frac{1}{N!\Lambda^{3N}} \int dr^N \exp\left\{-\beta\left[\Gamma(r^N) - \mu N + \sum_{i=1}^{N}\varphi(r_i)\right]\right\}. \quad (14)$$

Details are in Data S2. $\Omega = -(\ln\Xi)/\beta$ is the grand potential. According to PDFT, A is constructed, and the grand potential can be calculated accordingly $\Omega = A - \mu N$. Thus

$$\Omega = A - \mu N = F + \int dr\varphi(r)\rho(r) - \mu N$$
$$= F + \int dr[\varphi(r) - \mu]\rho(r) \quad (15)$$

The chemical potential is composed of ideal term and excess term,

$$\mu = \mu^{id} + \mu^{ex}, \quad (16)$$

where μ^{id} is calculated from $\mu^{id}(r) = \delta F^{id}/\delta\rho(r)$, and

$$\beta F^{id}[\rho_l(r)] = \sum_l \int dr\rho_l(r)\left[\ln(\rho_l(r)\Lambda^3) - 1\right]. \quad (17)$$
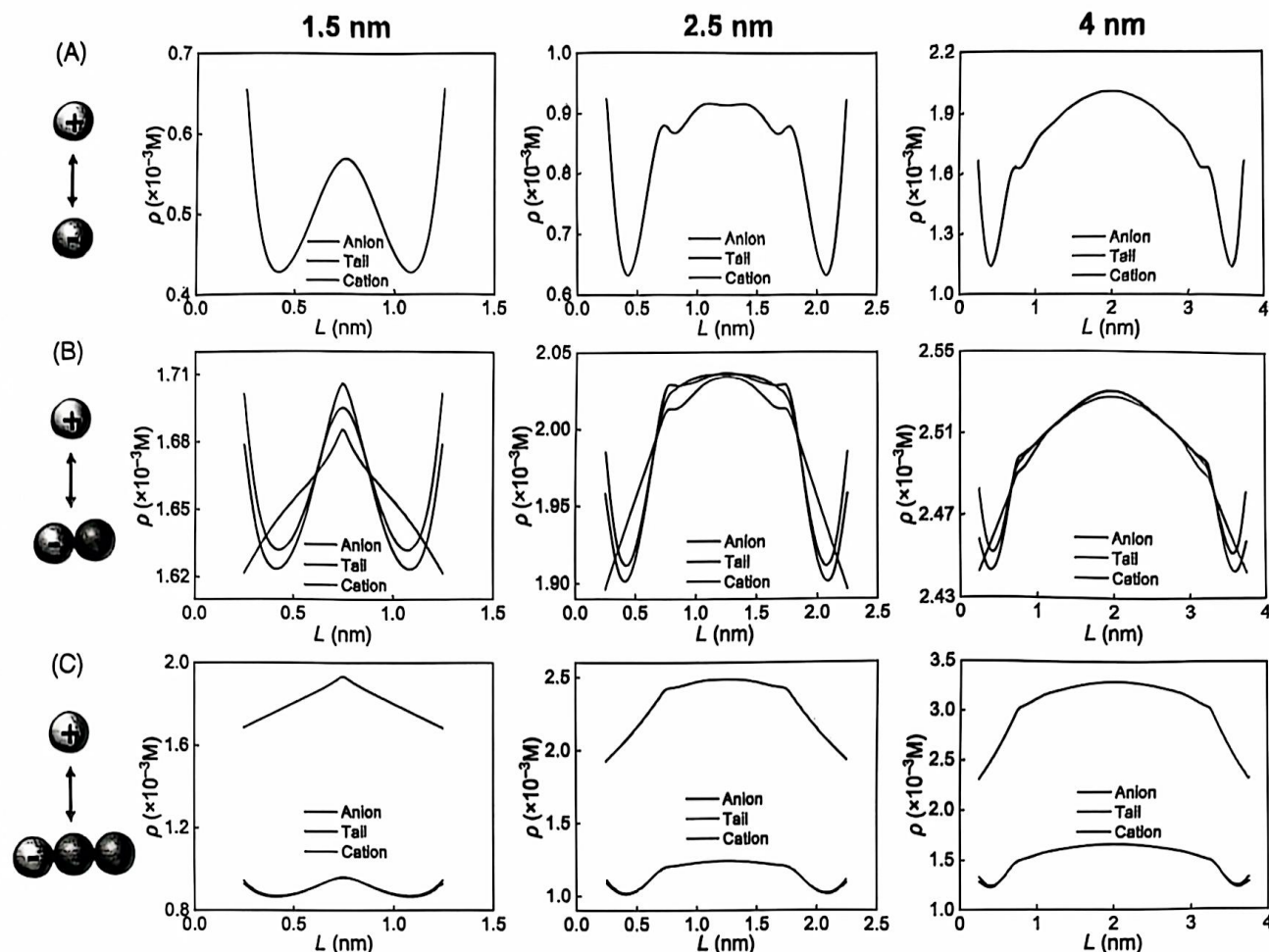
The μ^{ex} is calculated by Equation (6).

FIGURE 2 Density profiles of ionic fluids with (A) no tail chain, (B) one tail chain, and (C) two tail chains in three widths of slit pores, which are respectively 1.5, 2.5, and 4 nm, at $T^* = 0.05$ and $\rho_b = 0.0002$ M. Neutral tail chains tend to be distributed in the middle of slit pores.

3 | RESULTS AND DISCUSSION

3.1 | Density profile in confined space

To derive the phase equilibrium curve, it is necessary to calculate the density profiles of ionic fluids at various temperatures. Multiple concentrations are screened at each temperature, and the corresponding chemical potential and grand potential are derived to identify a pair of phase equilibrium points. Based on PDFT, the distribution of ionic fluids in confined spaces can be intuitively obtained. In the case of an ionic fluid consisting solely of a single cation and a single anion, the phase behavior in the bulk is commonly characterized in relation to the reduced temperature denoted as $T^* = 4\pi\varepsilon\varepsilon_0\sigma/(\beta e^2) = \sigma/l_B$. In this work, we selected a temperature of $T^* = 0.05$ and above. The specified condition pertains to an ionic liquid or organic electrolyte, which features an ion diameter of $\sigma = 0.5$ nm and temperature roughly around $T = 300$ K. Three ionic fluids in three widths of confined space (1.5, 2.5, and 4 nm) are calculated. Since each phase equilibrium point requires screening from many densities, multiple concentrations are calculated for each pair of phase equilibrium points. Figure 2 shows the density profiles of three ionic fluids at $T^* = 0.05$ and

$\rho_b = 0.0002$ M. The ionic density profiles show the depletion effect near a neutral wall. The density profile curve rises in the middle, indicating that ions tend to distribute in the bulk phase of the slit. For the model ionic system without a tail chain in a neutral slit pore (Figure 2A), the symmetry of the system results in identical density profiles for both cations and anions. The neutral tail chain tends to move away from the interface, so adding tail chains increases the density at the bulk phase compared to the interface (Figure 2B,C).

3.2 | Condition of phase equilibrium

Based on PDFT, we can derive the grand potential $\beta\Omega$ and chemical potential $\beta\mu$ of the ion system from Equations (15) and (16), respectively. If the grand potential and chemical potential of the vapor-like phase and the liquid-like phase are equal respectively at a temperature, the two phases reach equilibrium. To find the phase equilibrium point, a large number of ion densities at a temperature need to be calculated, and corresponding grand potential and chemical potential need to be derived from PDFT. The dependence curves of the grand potential and the chemical potential can be drawn, and the curves of
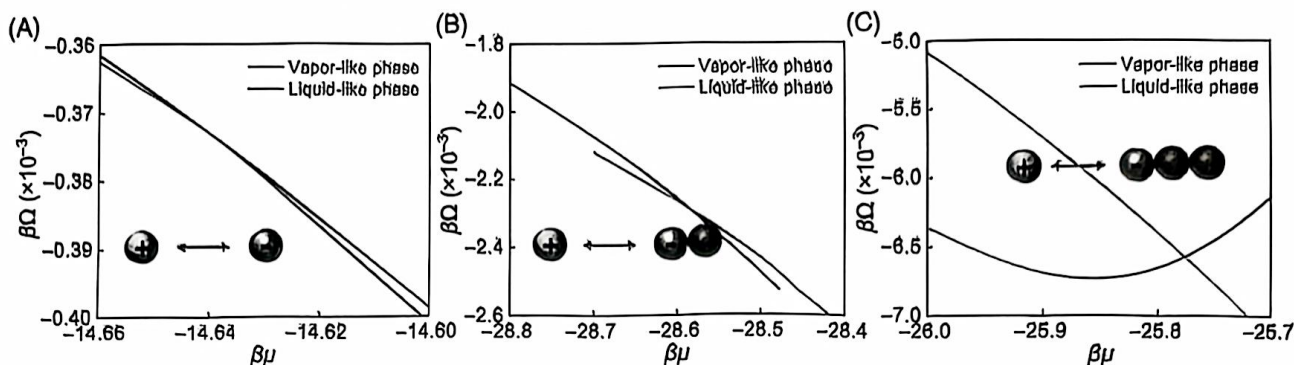
FIGURE 3 The grand potential $\beta\Omega$ of three ionic fluids [(A) no tail chain, (B) one tail chain, and (C) two tail chains] in the system is a function of the chemical potential $\beta\mu$, in an $H = 2.5$ nm pore at $T^* = 0.05$. The intersection point means that the corresponding vapor-like and liquid-like points reach phase equilibrium, and the corresponding two densities are a pair of equilibrium densities at the set temperature.

the vapor-like phase and the liquid-like phase are continuous, respectively. If two curves have an intersection point, the corresponding two densities are vapor-like and liquid-like phases coexisting in the pores. At a representative temperature of $T^* = 0.05$, Figure 3 presents the relationship between the grand potential $\beta\Omega$ and chemical potential $\beta\mu$ for three distinct ionic fluids within a pore of $H = 2.5$ nm. Generally, the grand potential decreases with the chemical potential. However, the curve undergoes a turning point in the liquid-like phase with longer chain lengths, which may be related to the longer tail chain. At high densities of liquid-like phases, longer tail chains bring more microstate numbers, and there are also more sample systems at each chemical potential. This means that more complex microstate states may also bring the same grand partition function (or grand potential energy). Therefore, due to the addition of tail chains, the complexity of the system increases, resulting in irregular changes in the grand partition function, and different chemical potentials may also bring the same grand potential energy (the emergence of minimum).

The critical point of the phase diagram can be determined by gradually increasing the temperature. By gradually calculating multiple densities at higher temperatures, the temperature at which the intersection point disappears in the Ω–μ diagram can be found. In addition, if the critical point needs to be precise enough, it can be gradually approached through the binary method.

3.3 | Phase diagram of confined ionic fluids

According to the phase equilibrium conditions, if the phase equilibrium point is found at various temperatures, the corresponding equilibrium density at each temperature can be plotted to obtain a phase diagram. Figure 4 shows the phase diagrams of three widths of confined spaces and bulk phase, which can intuitively discover the effect of fluid chain length on phase equilibrium. It can be found that ionic fluids without tail chains have the widest phase diagram and higher critical points. As the chain length increases, the phase diagram gradually narrows. The equilibrium density of the liquid-like phase decreased significantly, while the equilibrium density of the vapor-like phase increased but not significantly, almost overlapping. Prior

research[62] has indicated that the creation of pairs comprising oppositely charged ions modifies the effective interactions across all particles. This ion-pairing phenomenon leads to a reduced effective attraction between structural entities, consequently lowering the critical temperature associated with phase transition. It can be indirectly verified in Figure 4 that the addition of tail chains inevitably leads to a decrease in the interaction between anions and cations, which also leads to a narrowing of the phase diagram and a decrease in the critical point. In addition, in the vapor-like phase, the density of ionic species is low, and the interaction between them is weak, leading to the negligible impact of tail chains on the system. Therefore, the dependence of vapor-like phases on chain length is weak, and the critical point will shift left with the chain length.

In addition, the effect of confined space width on phase equilibrium was also observed. As shown in Figure 5, the red line corresponds to the coexistence curve in the bulk phase. Consistent with early theoretical research,[60,62] confinements narrow the coexistence envelope. The dependence of the vapor-like phase on the width of slit holes is weak. As the pore width decreases, the liquid-like phase curve significantly shifts to the left, consistent with previous research results.[42] Confinements also reduce the critical temperature. In narrow pores, the presence of ionic fluids can manifest in two distinct phases: a liquid-like phase or a vapor-like phase. The phase behavior relies on several factors including pore size, surface potential, temperature, and chemical potential of the ionic species. This phenomenon, known as capillary evaporation, is the response of ionic fluids to changes in external potential or thermodynamic conditions.

3.4 | Ionic fluid under confinement and electric field

Generally, the scene of ionic fluid in a confined space is mainly a porous electrode, often accompanied by a certain electric field. Ionic fluids are affected by both confinement and electric fields. The distribution of ionic fluids with a tail chain under various electric fields was studied. Select a slit width of 2.5 nm. As shown in Figure 6, select

FIGURE 4 Phase diagrams of three ionic fluids in confined spaces with widths of (A) 1.5 nm, (B) 2.5 nm, (C) 4 nm, and (D) bulk phase. Longer tail chains lead to narrower phase diagrams. The red star represents the critical point.
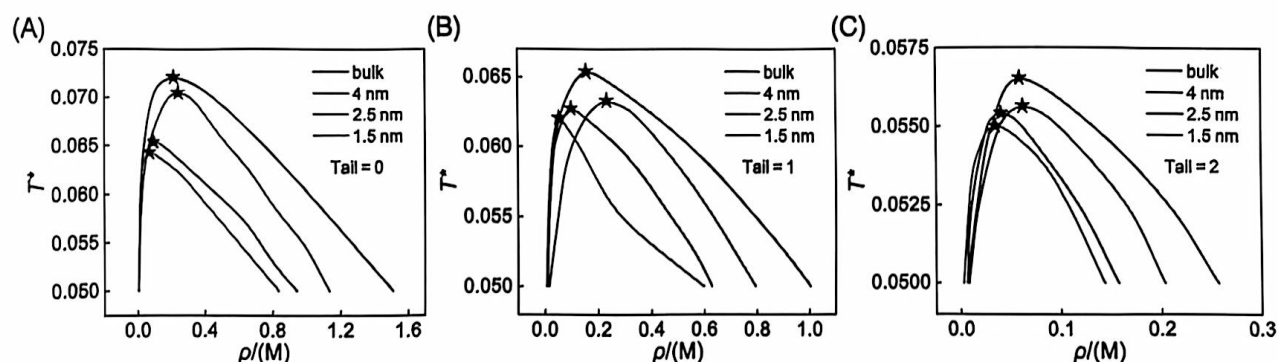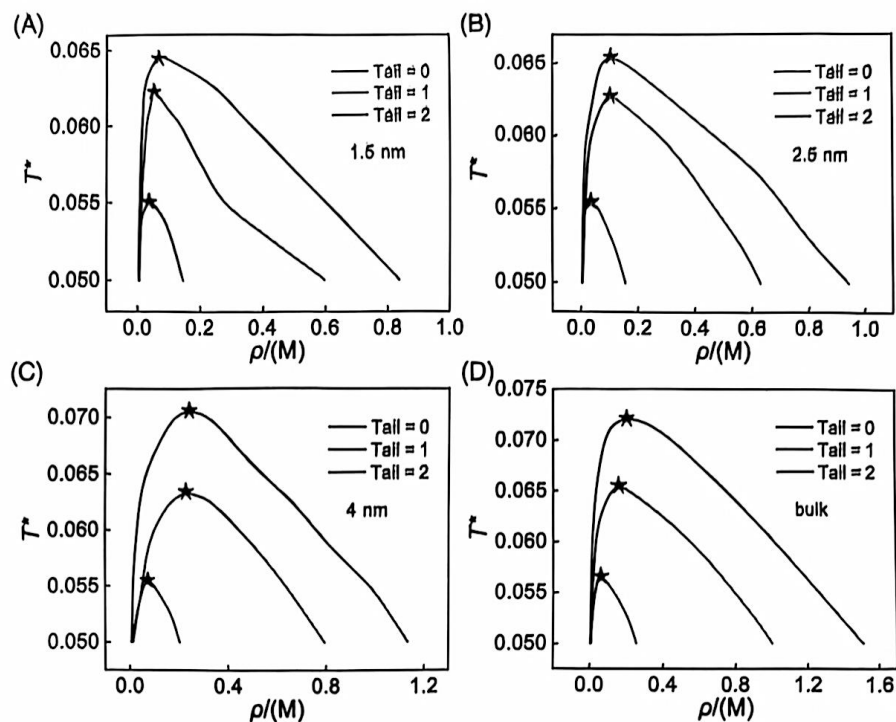

FIGURE 5 Phase diagrams of ionic fluids with (A) no tail chain, (B) one tail chain, and (C) two tail chains under various slit pore widths. Confinements lead to narrower phase diagrams and lower critical points. The red star represents the critical point.
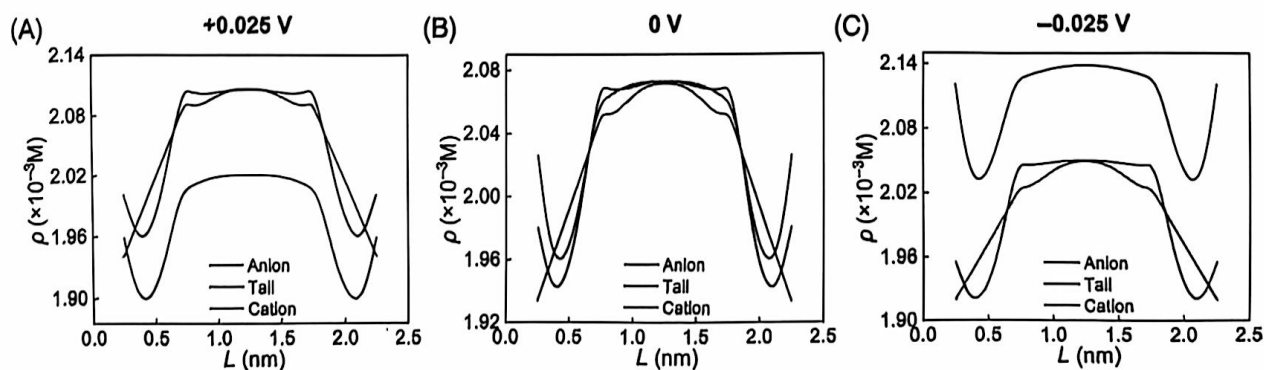

FIGURE 6 Density distribution of ionic fluid with one tail chain in a 2.5 nm wide slit pore at three potentials, which are (A) +0.025 V, (B) 0 V, and (C) −0.025 V, respectively.

three representative electric potentials and observe the density profile, which are +0.025, 0, and −0.025 V, respectively. In positively charged slit, anions along with tail chains will have a higher density due to the effect of electric potential. Negative charged slits produce the opposite phenomenon, with more cations present. Similar to the results in Section 3.1, ions also tend to be distributed in the middle of the slits. The electric field did not alter the distribution trend of species.

3.5 | Ionic fluid phase equilibrium in charged confinement

The phase behavior of ionic fluids with tail chains at six potentials was investigated. Similarly, the phase equilibrium points are selected by screening the equilibrium density according to the phase equilibrium conditions in Section 3.2. Each pair of phase equilibrium points requires screening dozens of densities. Figure 7 shows a phase diagram with a potential from −0.05 to 0.075 V. In the case of anions with tail chains, a positive potential widens the phase diagram, whereas a negative potential narrows it. From the density profile in Section 3.4, it can be found
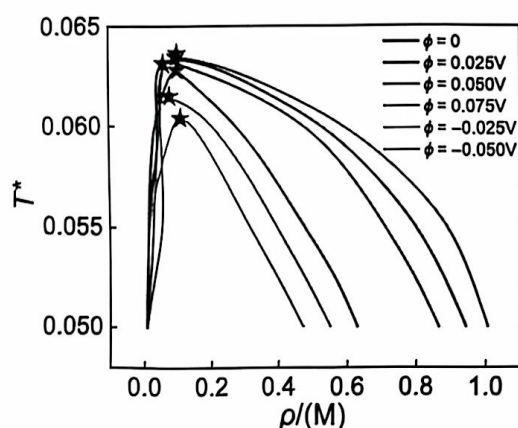
that positively charged slits attract more anions and their tail chains, resulting in a more complex situation in the slits, which may lead to more complex interactions, thereby widening the phase diagram. While negatively charged slits attract more cations and fewer anions with tail chains, resulting in simpler interactions and narrower phase diagrams. The application of a positive electric field force neutral tail chains, which prefer to stay in the center of the slit, to be dragged toward the wall by anions, thereby diminishing the dominant role of the volume exclusion effect in the central region of the slit. Due to the fact that the critical temperature has not decreased, and the volume exclusion effect is not strong enough, it manifests as an increase in ion concentration to form a liquid phase. Similarly, vapor-like phases are relatively insensitive to changes in electrical potential. Interestingly, the dependence of the density offset of the liquid-like phase on the potential seems to be regular.

3.6 | Dependence of phase diagram offset on electric potential

Due to the relative insensitivity of the vapor-like phase to the change in electric potential, the dependence of the density offset of the liquid-like phase on the electric potential is mainly explored. According to Figure 7, the offset appears to be linear. Therefore, to quantitatively explain the density shift, the difference between the density of the liquid-like phase and the density at zero potential at the same temperature is defined as the offset of the phase diagram $\Delta\rho$. The $\Delta\rho$ shown in Figure 8A is the offset at a potential of 0.025 V at $T^* = 0.055$. As shown in Figure 8B, a linear relationship can be found by plotting the dependence of the offset and potential difference at

FIGURE 7 The phase diagram of ionic fluid with a tail chain at six potentials. A positive electric potential shifts the liquid-like line to the right, and a negative electric potential shifts it to the left. The red star represents the critical point.

TABLE 1 The two parameters a and b in empirical Equation (18) were obtained by fitting at various temperatures and the corresponding R^2 and Pearson's r.

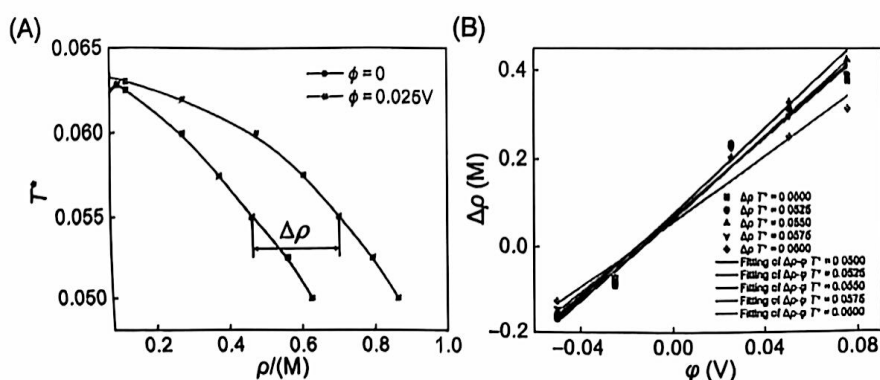| T^*	a	b	R^2	Pearson's r
0.0500	4.5933	0.0695	0.9770	0.9884
0.0525	4.7754	0.0642	0.9817	0.9908
0.0550	4.9078	0.0773	0.9886	0.9943
0.0575	4.4733	0.0722	0.9842	0.9921
Average	4.6875	0.0708		

FIGURE 8 (A) The offset of the phase diagram $\Delta\rho$ at a potential of 0.025 V at $T^* = 0.055$. (B) Fitting the correlation between offset and potential difference at multiple temperatures to find a linear relationship.

various temperatures. The determination coefficients R^2 of the fitting are all >0.97. The Pearson correlation coefficients (Pearson's r) are all >0.98, which confirms the strong linear relationship between offset and potential. We can obtain an empirical formula to predict the liquid-like phase density shift at various potentials.

$$\Delta\rho = a\varphi + b \quad (18)$$

where φ is the potential carried by the slit pore, the parameters a and b at various temperatures are shown in Table 1. Except for the temperature near the critical point, the parameters at other temperatures are remarkably close. $\bar{a} = 4.6875$ and $\bar{b} = 0.0708$ are available for any temperature. Through the calculation of PDFT, empirical prediction formulas for various chain lengths and slit widths can be obtained, facilitating the prediction of fluid phase behavior in complex situations.

4 | SUMMARY AND CONCLUSIONS

To summarize, PDFT is an effective tool for calculating fluid phase equilibria under complex conditions in chemical engineering. By deriving the grand potential and chemical potential of each species in the system, the phase equilibrium point corresponding to the temperature can be obtained. The phase behavior of ionic fluids in confined spaces with electric fields is described quantitatively, and empirical formulas are derived.

1. The improved associating PDFT accurately predicts the phase behavior of polymer fluids by incorporating both fluid chain connectivity and ion association.
2. The existence of fluid tail chains decreases intermolecular interactions and narrows the phase diagram. Confinements also narrow the phase diagram. The dependence of the vapor-like phase on chain length and slit is weak. The equilibrium density of the liquid-like phase decreases significantly with chain length.
3. A positive potential widens the phase diagram, whereas a negative potential narrows it. Similarly, vapor-like phases exhibit limited sensitivity to variations in electrical potential.
4. The relationship between the density offset of the liquid-like phase and the electric potential was examined, revealing a linear correlation. Based on this finding, an empirical formula was derived to predict the density offset under various electric potentials.

Importantly, PDFT is an efficient tool for predicting fluid phase behavior, which has an extremely broad industrial application prospect in the electrode-electrolyte interface. This work aims to inspire future experimental and theoretical efforts in fluid interfaces chemical engineering.

AUTHOR CONTRIBUTIONS

Jin Cheng: Conceptualization (equal); data curation (equal); formal analysis (lead); investigation (lead); methodology (equal); software (lead); validation (lead); visualization (lead); writing – original draft (lead). Jipeng Xu: Visualization (supporting); writing – review and editing (equal). Sijie Wang: Visualization (supporting); writing – review and editing (equal). Xueqian Chen: Resources (equal); supervision (supporting). Cheng Lian: Conceptualization (lead); methodology (lead); project administration (lead); resources (equal); supervision (lead); writing – review and editing (supporting). Honglai Liu: Funding acquisition (equal); project administration (equal); resources (equal); supervision (supporting).

DATA AVAILABILITY STATEMENT
The numerical data from Figures 2 to 8 is available in the Data S1 file.

ORCID
Cheng Lian ⓘ https://orcid.org/0000-0002-9016-832X

REFERENCES

1. Xu J, Zhang J, Pollard TP, et al. Electrolyte design for Li-ion batteries under extreme operating conditions. *Nature.* 2023;614(7949):694-700.
2. Choi N-S, Chen Z, Freunberger SA, et al. Challenges facing lithium batteries and electrical double-layer capacitors. *Angew Chem Int Ed.* 2012;51(40):9994-10024.
3. Yi E, Shen X, Chen X, et al. Preparation of biomass composite activated carbon based supercapacitor materials and their application in energy storage devices. *Chem Eng Sci.* 2023;282:119193.
4. Lian C, Cheng J, Huang P, Tao H, Yang J, Liu H. Thermodynamics of new energy chemical engineering. *Chem Ind Eng Prog.* 2021;40(9): 4711-4733.
5. Hayashi T. Water at interfaces: its behavior and roles in interfacial phenomena. *Chem Lett.* 2021;50(6):1173-1180.
6. Cheng J, Zhou W, Zhu M, et al. Optimizing microstructure of polyelectrolyte ion exchange membrane for electrodialysis. *Chem Eng J.* 2023;468:143669.
7. Hao G, LI E, LI J-X, et al. A deep learning perspective on electrohydrodynamic micro-droplet interface deformation characteristics. *Chem Eng Sci.* 2023;276:118772.
8. Nielsen M, Björketun ME, Hansen MH, Rossmeisl J. Towards first principles modeling of electrochemical electrode–electrolyte interfaces. *Surf Sci.* 2015;631:2-7.
9. Sakaushi K, Kumeda T, Hammes-Schiffer S, Melander MM, Sugino O. Advances and challenges for experiment and theory for multi-electron multi-proton transfer at electrified solid–liquid interfaces. *Phys Chem Chem Phys.* 2020;22(35):19401-19442.
10. Lück J, Latz A. The electrochemical double layer and its impedance behavior in lithium-ion batteries. *Phys Chem Chem Phys.* 2019;21(27): 14753-14765.
11. Tao H, Lian C, Liu H. Multiscale modeling of electrolytes in porous electrode: from equilibrium structure to non-equilibrium transport. *Green Energy Environ.* 2020;5(3):303-321.

12. Liu C, Ling Y, Wang Z, Zheng W, Sun W, Zhao L. Unveiling the micro-environments between ionic liquids and methanol for alcoholysis of poly(ethylene terephthalate). *Chem Eng Sci.* 2022;247:117024.

13. Han W, Liu Y, Meng W, Wang L, Liu S. Dendrite-free and gasless potassium metal anodes assisted by the mechanical-electrochemical enhancing solid K-electrode and electrolyte interface. *Chem Eng Sci.* 2023;282:119295.

14. Li M, Hu Y, Lv L, et al. Implementation of solvation free energy framework to predict the vapor-liquid equilibrium behaviors for the water-hydrazine and ethanol-water azeotropic systems. *Chem Eng Sci.* 2023;275:118751.

15. Sun G, Zhao Z, Sun S, Ma Y, Li H, Gao X. Vapor-liquid phase equilibria behavior prediction of binary mixtures using machine learning. *Chem Eng Sci.* 2023;282:119358.

16. Tao H, Chen G, Lian C, Liu H, Coppens M-O. Multiscale modeling of ion transport in porous electrodes. *AIChE J.* 2022;68(4):e17571.

17. Kawase M, Sato K, Mitsui R, et al. Electrochemical reaction engineering of polymer electrolyte fuel cell. *AIChE J.* 2017;63(1):249-256.

18. Cheng J, Tao H, Ma K, et al. A theoretical model for the charging dynamics of associating ionic liquids. *Front Chem Eng.* 2022;4:852070.

19. Kiyohara K, Sugino T, Asaka K. Phase transition in porous electrodes. *J Chem Phys.* 2011;134(15):154710.

20. Kiyohara K, Shioyama H, Sugino T, Asaka K. Phase transition in porous electrodes. II. Effect of asymmetry in the ion size. *J Chem Phys.* 2012;136(9):094701.

21. Ruiz-Cabello FJM, Maroni P, Borkovec M. Direct measurements of forces between different charged colloidal particles and their prediction by the theory of Derjaguin, Landau, Verwey, and Overbeek (DLVO). *J Chem Phys.* 2013;138(23):234705.

22. Kondrat S, Wu P, Qiao R, Kornyshev AA. Accelerating charging dynamics in subnanometre pores. *Nat Mater.* 2014;13(4):387-393.

23. Jäckel N, Simon P, Gogotsi Y, Presser V. Increase in capacitance by subnanometer pores in carbon. *ACS Energy Lett.* 2016;1(6):1262-1265.

24. He Y-L, Liu Q, Li Q, Tao W-Q. Lattice Boltzmann methods for single-phase and solid-liquid phase-change heat transfer in porous media: a review. *Int J Heat Mass Transfer.* 2019;129:160-197.

25. Batalin OY, Vafina NG. Global transformation of fluid structure and corresponding phase behavior. *J Supercrit Fluids.* 2023;203:106081.

26. Halperin A, Kröger M, Winnik FM. Poly(N-isopropylacrylamide) phase diagrams: fifty years of research. *Angew Chem Int Ed.* 2015;54(51):15342-15367.

27. Matsen MW. Effect of architecture on the phase behavior of AB-type block copolymer melts. *Macromolecules.* 2012;45(4):2161-2165.

28. Wang S, Shen Y. CFD-DEM-VOF-phase diagram modelling of multi-phase flow with phase changes. *Chem Eng Sci.* 2023;273:118651.

29. Królikowska M, Królikowski M, Domańska U. Effect of cation structure in quinolinium-based ionic liquids on the solubility in aromatic sulfur compounds or heptane: thermodynamic study on phase diagrams. *Molecules.* 2020;25(23):5687.

30. Shen C, Li C-X, Li X-M, Lu Y-Z, Muhammad Y. Estimation of densities of ionic liquids using Patel-Teja equation of state and critical properties determined from group contribution method. *Chem Eng Sci.* 2011;66(12):2690-2698.

31. Blesic M, Lopes JNC, Pádua AAH, Shimizu K, Gomes MFC, Rebelo LPN. Phase equilibria in ionic liquid-aromatic compound mixtures, including benzene fluorination effects. *J Phys Chem B.* 2009;113(21):7631-7636.

32. Yan L. Electrostatic correlations: from plasma to biology. *Rep Prog Phys.* 2002;65:1577-1632.

33. Lu H, Li B, Nordholm S, Woodward CE, Forsman J. Ion pairing and phase behaviour of an asymmetric restricted primitive model of ionic liquids. *J Chem Phys.* 2016;145(23):234510.

34. Yan Q, Liu H, Hu Y. Simulation of phase equilibria for lattice polymers. *Macromolecules.* 1996;29(11):4066-4071.

35. Jiang J, Yan Q, Liu H, Hu Y. Monte Carlo simulations of liquid-liquid equilibria for ternary chain molecule systems on a lattice. *Macromolecules.* 1997;30(26):8459-8462.

36. Fantoni R, Pastore G. Monte Carlo simulation of the nonadditive restricted primitive model of ionic fluids: Phase diagram and clustering. *Phys Rev E.* 2013;87(5):052303.

37. Yang J, Peng C, Liu H, Hu Y. Liquid-liquid equilibria of polymer solutions with oriented interactions. *Fluid Phase Equilibr.* 2006;249(1):192-197.

38. Yang J, Peng C, Liu H, Hu Y. Calculation of vapor-liquid and liquid-liquid phase equilibria for systems containing ionic liquids using a lattice model. *Ind Eng Chem Res.* 2006;45(20):6811-6817.

39. Xu X, Peng C, Liu H, Hu Y. Modeling pVT properties and phase equilibria for systems containing ionic liquids using a new lattice-fluid equation of state. *Ind Eng Chem Res.* 2009;48(24):11189-11201.

40. Jiang J, Prausnitz JM. Phase equilibria for chain-fluid mixtures near to and far from the critical region. *AIChE J.* 2000;46(12):2525-2536.

41. Kondrat S, Bier M, Harnau L. Phase behavior of ionic liquid crystals. *J Chem Phys.* 2010;132(18):184901.

42. Liu K, Zhang P, Wu J. Does capillary evaporation limit the accessibility of nonaqueous electrolytes to the ultrasmall pores of carbon electrodes? *J Chem Phys.* 2018;149(23):234708.

43. Liu K, Wu J. Wettability of ultra-small pores of carbon electrodes by size-asymmetric ionic fluids. *J Chem Phys.* 2020;152(5):054708.

44. Cheng J, Li J-H, Lian C, Liu H. Development and application of fluid density functional theory for novel electrochemical interfaces. *Curr Opin Chem Eng.* 2023;41:100946.

45. Yang J, Lian C, Liu H. Chain length matters: structural transition and capacitance of room temperature ionic liquids in nanoporous electrodes. *Chem Eng Sci.* 2020;227:115927.

46. Cheng J, Xu J, Yang J, Lv W, Lian C, Liu H. Enhanced oil recovery by sacrificing polyelectrolyte to reduce surfactant adsorption: a classical density functional theory study. *Chem Eng Sci.* 2022;261:117957.

47. Wu J. Density functional theory for chemical engineering: from capillarity to soft materials. *AIChE J.* 2006;52(3):1169-1193.

48. Fu J, Tian Y, Wu J. Classical density functional theory for methane adsorption in metal-organic framework materials. *AIChE J.* 2015;61(9):3012-3021.

49. Xu J, Cheng J, Yang J, et al. The charge regulation of surfactants on the rock surface in nanoconfinement: a reaction-coupling fluid density functional theory study. *Chem Eng Sci.* 2023;275:118718.

50. Jiang D-E, Meng D, Wu J. Density functional theory for differential capacitance of planar electric double layers in ionic liquids. *Chem Phys Lett.* 2011;504(4):153-158.

51. Wu J, Jiang T, Jiang D-e, Jin Z, Henderson D. A classical density functional theory for interfacial layering of ionic liquids. *Soft Matter.* 2011;7(23):11222-11231.

52. Wu J. Understanding the electric double-layer structure, capacitance, and charging dynamics. *Chem Rev.* 2022;122(12):10821-10859.

53. Kumaravadivel R, Evans R. Calculations of the surface energy of simple liquid metals. *J Phys C: Solid State Phys.* 1975;8(6):793-808.

54. van Roij R, Dijkstra M, Hansen J-P. Phase diagram of charge-stabilized colloidal suspensions: van der Waals instability without attractive forces. *Phys Rev E.* 1999;59(2):2010-2025.

55. Wertheim MS. Fluids with highly directional attractive forces. I. Statistical thermodynamics. *J Stat Phys.* 1984;35(1):19-34.

56. Li Z, Wu J. Density functional theory for planar electric double layers: closing the gap between simple and polyelectrolytes. *J Phys Chem B.* 2006;110(14):7473-7484.

57. Li Z, Wu J. Density functional theory for polyelectrolytes near oppositely charged surfaces. *Phys Rev Lett.* 2006;96(4):048302.

58. Yu Y-X, Wu J. A fundamental-measure theory for inhomogeneous associating fluids. *J Chem Phys.* 2002;116(16):7094-7103.

59. Ebeling W, Grigo M. Mean spherical approximation-mass action law theory of equilibrium and conductance in ionic solutions. *J Solution Chem.* 1982;11(3):151-167.
60. Holovko M, Patsahan T, Patsahan O. Effects of disordered porous media on the vapour-liquid phase equilibrium in ionic fluids: application of the association concept. *J Mol Liq.* 2017;228:215-223.
61. Olaussen K, Stell G. New microscopic approach to the statistical mechanics of chemical association. *J Stat Phys.* 1991;62(1): 221-237.
62. Pizio O, Sokołowski S. Phase behavior of the restricted primitive model of ionic fluids with association in slitlike pores. Density-functional approach. *J Chem Phys.* 2005;122(14):144707.

SUPPORTING INFORMATION

Additional supporting information can be found online in the Supporting Information section at the end of this article.